

Jahn-Teller induced Berry phase in spin-orbit coupled Bose-Einstein condensates

Jonas Larson¹ and Erik Sjöqvist²
¹*NORDITA, 106 91 Stockholm, Sweden*
²*Department of Quantum Chemistry,
 Uppsala University, Box 518,
 Se-751 20 Uppsala, Sweden*
 (Dated: February 12, 2022)

We demonstrate that Berry phases may greatly affect the dynamics of spin-orbit coupled Bose-Einstein condensates. The effective model Hamiltonian under consideration is shown to be equivalent to the $E \times \varepsilon$ Jahn-Teller model first introduced in molecular physics. The corresponding conical intersection is identified and the Berry phase acquired for a wave packet encircling the intersection studied. It is found that this phase manifests itself in the density profile of the condensate, making it a directly measurable quantity via time-of-flight detection. Moreover, the non-Abelian gauge structure of the system is addressed and we verify how it affects the dynamics.

PACS numbers: 03.75.Nt, 03.65.Vf, 71.70.Ej

I. INTRODUCTION

The realization of Bose-Einstein condensates [1] opened a new door for the study of quantum phenomena. Since then the field has seen a tremendous progress in terms of trapping, cooling and manipulating atoms, covering cold atoms in optical lattices [2], BCS-BEC crossover [3] and multi-component Bose-Einstein condensates [4]. Moreover, it has been demonstrated both theoretically [5, 6] and experimentally [7] that ultracold multi-level atoms moving in spatially dependent laser fields give rise to effective gauge potentials. Considering four-level atoms in a tripod setup, non-Abelian gauge fields are achieved [8]. The idea of utilizing a four-level atom with three degenerate ground states coupled to one excited state to generate non-Abelian gauge potentials dates back to the work of Unanyan and co-workers [9], where however the effective magnetic fields arise from time-dependence of the Hamiltonian rather than spatial dependence. The particular system configuration of Ref. [8] has turned out to be extremely rich, and a series of papers investigating various aspects of the model have been published recently. Among these are, spin-Hall effects [10], the Aharonov-Bohm effect [11], relativistic characteristics [12, 13], spin-echo phenomena of trapped fermions [14], spin dynamics [15], expansion to time-dependent laser fields [16], novel phases of the condensate [17], the structure of the energy spectrum [18], and effective magnetic monopoles [19].

For certain laser arrangements, the energy dispersions possess a point-degeneracy also termed *conical intersection* (CI) [20]. It is well known [21, 22] that apart from the dynamical phase, encircling a CI renders a Berry phase of the state vector [23]. Differing from typical situations in molecular and chemical physics, here the CI occurs in momentum and not in position space. As a consequence, the Berry phase is more directly manifested in the momentum wave function. Similar situations appear in graphene [24] and cold atoms in elaborate optical lattice configurations [25].

In the current work, we consider a harmonically trapped spinor Bose-Einstein condensate in the presence of spatially dependent laser fields such that a CI is recovered in momentum space. By taking the harmonic confinement of the condensate into account, the resulting Hamiltonian is equivalent to the $E \times \varepsilon$ Jahn-Teller one [26], but with position and momentum interchanged. Moreover, the non-linear terms arising from atom-atom scattering are included. Such terms are absent in for example CI-models in molecular physics [20, 27, 28]. Utilizing numerical wave packet simulations, we thoroughly discuss the Berry phase and how it affects the system dynamics, both on a short and long time scale. It is found that over longer time periods, the population of the two phonon modes is swapped, and in particular, the characteristics of this exchange mechanism depend on the Berry phase. Various studies have been concerned about Berry phases in Bose-Einstein condensates influenced by slowly varying external fields [29, 30]. Contrary to these references, in the present model the Berry phase shows up in the internal spinor dynamics as an effective spatially dependent gauge field, in analogy with the Born-Oppenheimer scenario in molecular theory [21]. We note that Berry phases were as well considered in Refs. [11, 13], but without taking into account for a trapping potential nor atom-atom collisions. A harmonic trapping potential causes the momentum wave packet to spread, which has important consequences for its dynamics. In addition to investigating the consequences of a non-zero Berry phase, we also study the non-Abelian structure of the system. We show that one round-trip of the CI clockwise or anti-clockwise brings about different final states.

The paper is outlined as follows. In the next section, the model system is introduced and the effective Gross-Pitaevskii equation given. The equivalence with the $E \times \varepsilon$ Jahn-Teller Hamiltonian is demonstrated and we discuss the form of the momentum potential energy surfaces. Section III is devoted to numerical simulations. First, in Sec. III A, the short time evolution is consid-

ered, the non-cyclic Berry phase [31] for the spinor state is computed, the impact of the Berry phase on the wave packet dynamics is clarified, and we show how a time-of-flight measurement of the condensate would reveal the presence of a Berry phase. The following Sec. III B deals with the long time scale properties. A collapse-revival as well as a swapping phenomena is found. The underlying non-Abelian structure is envisaged in Sec. III C. Last we finish with concluding remarks in Sec. IV.

II. MODEL SYSTEM

We begin by deriving the effective single atom Hamiltonian, and then turn to the many-body case by including atom-atom scattering to obtain a mean field Gross-Pitaevskii equation.

The setup is detailed in Fig. 1 (a). Three degenerate meta stable Zeeman ground states are dipole coupled to an excited state via three respective external lasers. Using the notations of the figure and imposing the rotating wave approximation, the interaction Hamiltonian reads

$$H_I = \hbar\Delta|0\rangle\langle 0| + \hbar(\Omega_1|0\rangle\langle 1| + \Omega_2|0\rangle\langle 2| + \Omega_3|0\rangle\langle 3| + \text{h.c.}), \quad (1)$$

which defines the full Hamiltonian $H = \tilde{p}^2/(2m) + H_I$, \tilde{p} and m being the momentum and mass, respectively, of the atom. The coupling strengths, being proportional to the laser amplitudes, are parameterized as $\Omega_1 = \Omega \sin \theta \cos \varphi e^{iS_1}$, $\Omega_2 = \Omega \sin \theta \sin \varphi e^{iS_2}$ and $\Omega_3 = \Omega \cos \theta e^{iS_3}$ with $\Omega = \sqrt{|\Omega_1|^2 + |\Omega_2|^2 + |\Omega_3|^2}$. Here, θ , φ and S_i are allowed to be spatially dependent. The interaction part H_I of the full Hamiltonian may be readily diagonalized, rendering the eigenstates $|w_0\rangle$, $|w_3\rangle$, $|u_1\rangle$, and $|u_2\rangle$, where in particular the two states

$$\begin{aligned} |u_1\rangle &= \frac{1}{\sqrt{2}} \left(\left[\sin \varphi e^{i\pi/4} + \cos \theta \cos \varphi e^{-i\pi/4} \right] e^{-iS_{13}} |1\rangle \right. \\ &\quad \left. - \left[\cos \varphi e^{i\pi/4} - \cos \theta \sin \varphi e^{-i\pi/4} \right] e^{-iS_{23}} |2\rangle \right. \\ &\quad \left. - \sin \theta e^{-i\pi/4} |3\rangle \right), \\ |u_2\rangle &= \frac{1}{\sqrt{2}} \left(\left[\cos \theta \cos \varphi e^{-i\pi/4} - \sin \varphi e^{i\pi/4} \right] e^{-iS_{13}} |1\rangle \right. \\ &\quad \left. + \left[\cos \varphi e^{i\pi/4} + \cos \theta \sin \varphi e^{-i\pi/4} \right] e^{-iS_{23}} |2\rangle \right. \\ &\quad \left. - \sin \theta e^{-i\pi/4} |3\rangle \right), \end{aligned} \quad (2)$$

are degenerate with zero eigenvalue, and here $S_{ij} = S_i - S_j$. These two states are termed *dark states* as they do not couple to the excited state $|0\rangle$ via H_I . Due to the shifted energy of the remaining two states $|w_0\rangle$ and $|w_3\rangle$ compared to $|u_1\rangle$ and $|u_2\rangle$, they can be adiabatically

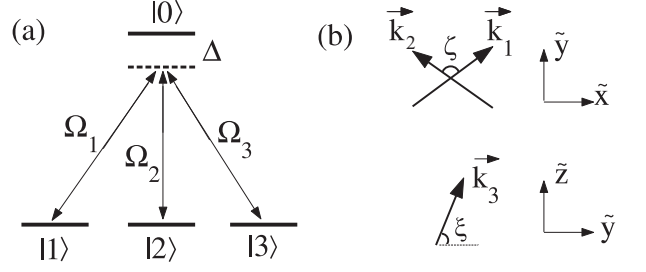


FIG. 1: Atomic (a) and laser (b) configurations.

eliminated from the Hamiltonian provided that $\Delta \gg \Omega$, ending up with an effective two-level problem for $|u_1\rangle$ and $|u_2\rangle$.

Before writing down the resulting Hamiltonian we specify the laser configurations [14], see Fig. 1 (b). First we assume $S_1 = S_2$, $S_{31} = mv_s \tilde{y}/\hbar$ and $\varphi = mv_\varphi \tilde{x}/\hbar$ and $\theta \in [0, \pi]$ some constant. Two lasers, which govern the coupling of $|1\rangle$ and $|2\rangle$ to $|0\rangle$, are propagating along \vec{k}_1 and \vec{k}_2 in the $\tilde{x}\tilde{y}$ -plane, where the angle of intersection between them is ζ . In the \tilde{x} -direction, these two lasers are standing waves, however mutually shifted in phase by $\pi/2$, and propagating waves in the \tilde{y} -direction. A third laser is a propagating wave along \vec{k}_3 in the $\tilde{y}\tilde{z}$ -plane, whose direction is determined by the angle ξ relative the \tilde{y} -axis. In terms of the angles ζ and ξ and the wave numbers $k_i = |\vec{k}_i|$ we have

$$\begin{aligned} S_1 &= S_2 = k_1 \tilde{y} \cos(\zeta/2), \\ S_3 &= k_3 \tilde{y} \cos \xi, \\ \varphi &= 2k_1 \tilde{x} \sin(\zeta/2). \end{aligned} \quad (3)$$

After the adiabatic elimination, the effective single particle two-level Hamiltonian becomes [14]

$$H_{\text{eff}} = \frac{\tilde{p}^2}{2m} + \delta_0 \hat{\sigma}_y - \tilde{v}_0 \hat{\sigma}_x \tilde{p}_{\tilde{x}} - \tilde{v}_1 \hat{\sigma}_y \tilde{p}_{\tilde{y}}, \quad (4)$$

where δ_0 is an effective Zeeman splitting, $\tilde{v}_0 = v_\varphi \cos \theta$, $\tilde{v}_1 = v_s \sin^2 \theta/2$ and $\hat{\sigma}_i$, with $i = x, y, z$ are the Pauli operators $\hat{\sigma}_x = |u_1\rangle\langle u_2| + |u_2\rangle\langle u_1|$, $\hat{\sigma}_y = -i|u_1\rangle\langle u_2| + i|u_2\rangle\langle u_1|$, and $\hat{\sigma}_z = |u_1\rangle\langle u_1| - |u_2\rangle\langle u_2|$. The \tilde{p} -dependence of the last two terms originates from non-adiabatic couplings [32], and we note that these do not include \tilde{p}_z and we may therefore factor out the \tilde{z} -dependence. The spin-orbit coupling is on a *Rashba*-form [33], which has been frequently studied in the context of semiconductor quantum-dots [34, 35].

We will further add a harmonic trapping potential (associated with angular frequency ω) for the atoms. This was in fact also done in Ref. [35]. However, for the condensate considered in this work, such a trapping potential is almost exclusively present in experiments, while this is not the case for the electrons in semiconducting quantum-dots of Ref. [35]. By properly Stark shifting

the internal atomic states, individual trapping potentials can be achieved. In particular, for certain constant Stark shifts, the Zeeman splitting term in the Hamiltonian [11, 14] can be made to vanish, which we will assume in the following. It should be mentioned that in order to justify adiabatic elimination of the two dark states, once the harmonic trapping potential has been included, one should assume not only $\Delta \gg \Omega$, but also $\Omega \gg \omega$ in order to ensure the validity of the Born-Oppenheimer separation.

Imposing s -wave scattering between the atoms in terms of the regular non-linear term gives a Gross-Pitaevskii equation. Defining the spinor wave function

$$\tilde{\Psi}(\tilde{x}, \tilde{y}, t) = \begin{bmatrix} \langle \tilde{x}, \tilde{y} | u_1 | \tilde{\Psi}(t) \rangle \\ \langle \tilde{x}, \tilde{y} | u_2 | \tilde{\Psi}(t) \rangle \end{bmatrix} = \begin{bmatrix} \tilde{\psi}_1(\tilde{x}, \tilde{y}, t) \\ \tilde{\psi}_2(\tilde{x}, \tilde{y}, t) \end{bmatrix}, \quad (5)$$

where $\psi_i(\tilde{x}, \tilde{y}, t) = \langle \tilde{x}, \tilde{y} | \psi_i(t) \rangle$, $i = 1, 2$ and the normalization reads $\int d\tilde{x} d\tilde{y} |\tilde{\Psi}(\tilde{x}, \tilde{y}, t)|^2 = 1$, the Gross-Pitaevskii equation takes the form

$$\begin{aligned} i\hbar \frac{\partial}{\partial t} \tilde{\Psi}(\tilde{x}, \tilde{y}, t) = & \left[-\frac{\hbar^2}{2m} \left(\frac{\partial^2}{\partial \tilde{x}^2} + \frac{\partial^2}{\partial \tilde{y}^2} \right) + \frac{m\omega^2}{2} (\tilde{x}^2 + \tilde{y}^2) \right. \\ & - i\hbar \tilde{v}_0 \boldsymbol{\sigma}_x \frac{\partial}{\partial \tilde{x}} - i\hbar \tilde{v}_1 \boldsymbol{\sigma}_y \frac{\partial}{\partial \tilde{y}} \\ & \left. + \tilde{\Psi}^\dagger(\tilde{x}, \tilde{y}, t) \mathbf{g} \tilde{\Psi}(\tilde{x}, \tilde{y}, t) \right] \tilde{\Psi}(\tilde{x}, \tilde{y}, t), \end{aligned} \quad (6)$$

where $\boldsymbol{\sigma}_i$ are the standard Pauli matrices acting on the spinor space and

$$\mathbf{g} = \begin{bmatrix} \tilde{g}_{11} & \tilde{g}_{12} \\ \tilde{g}_{12} & \tilde{g}_{22} \end{bmatrix} \quad (7)$$

is the matrix valued scattering amplitude. In general, the scattering amplitudes \tilde{g}_{11} , \tilde{g}_{22} and \tilde{g}_{12} can be different. We will in the following assume $\tilde{g}_{11} = \tilde{g}_{22} = \tilde{g}$ and $\tilde{g}_{12} = 0$, a condition that is supposed to be approximately achievable for a ^{87}Rb condensate [6]. We have numerically verified, using a non-zero \tilde{g}_{12} does not give rise to any qualitative changes of our results. In terms of physical quantities, $\tilde{g} = 4\pi\hbar^2 Na/mV$, where N is the number of condensate atoms, V the effective volume and a the s -wave scattering length. Attractive atom-atom interaction is obtained for $\tilde{g} < 0$ and repulsive for $\tilde{g} > 0$. Noteworthy is that the parameter \tilde{g} may be tuned over a wide range of values using Feshbach resonance techniques [36].

The single particle Hamiltonian Eq. (4), once the harmonic trapping potential has been included, is equivalent to the $E \times \varepsilon$ Jahn-Teller one, which was first introduced in molecular physics [26]. However, the canonical momentum and position variables are interchanged in the original $E \times \varepsilon$ Hamiltonian. Mathematically this is just a question of representations, but it has physical consequences, for example in state preparation and measurement. Another outcome of this is that the effect of the Berry phase normally apparent in the physical state $\tilde{\Psi}(\tilde{x}, \tilde{y}, t)$ will instead manifest itself in the spinor wave

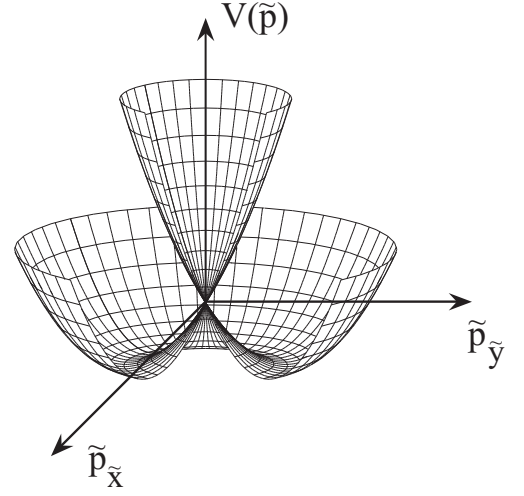


FIG. 2: Effective APS corresponding to the Gross-Pitaevskii equation (6). The conical intersection is located at the origin, $\tilde{p}_x = \tilde{p}_y = 0$, where the two APS become degenerate. Here we have $\tilde{v}_0 = \tilde{v}_1$.

function $\tilde{\Phi}(\tilde{p}_x, \tilde{p}_y, t)$ in the momentum representation, $\tilde{\Phi}$ being related to $\tilde{\Psi}$ via the Fourier transform

$$\tilde{\Phi}(\tilde{p}_x, \tilde{p}_y, t) = \int d\tilde{x} d\tilde{y} e^{-i(\tilde{x}\tilde{p}_x + \tilde{y}\tilde{p}_y)/\hbar} \tilde{\Psi}(\tilde{x}, \tilde{y}, t). \quad (8)$$

The phenomena we are studying are therefore more conveniently extracted by analyzing the problem in a momentum representation, and in particular in terms of an effective momentum-dependent potential.

For this purpose we introduce the unitary adiabatic transformation $U_{\text{ad}} = U_{\text{ad}}(\tilde{p}_x, \tilde{p}_y)$ that diagonalizes the spin-orbit term, namely

$$\begin{aligned} U_{\text{ad}} \begin{bmatrix} 0 & \tilde{v}_0 \tilde{p}_x - i\tilde{v}_1 \tilde{p}_y \\ \tilde{v}_0 \tilde{p}_x + i\tilde{v}_1 \tilde{p}_y & 0 \end{bmatrix} U_{\text{ad}}^\dagger \\ = \sqrt{(\tilde{v}_0 \tilde{p}_x)^2 + (\tilde{v}_1 \tilde{p}_y)^2} \boldsymbol{\sigma}_z \equiv \lambda \boldsymbol{\sigma}_z. \end{aligned} \quad (9)$$

This results in the effective adiabatic potential surfaces (APS) in momentum space, defined as

$$V_{\text{ad}}^\pm = \frac{1}{2m} (\tilde{p}_x^2 + \tilde{p}_y^2) \pm \lambda \quad (10)$$

which conically intersect at $\tilde{p} = 0$. Encircling the conical intersection (CI) gives rise to a Berry phase [23], which, indeed, is related to the gauge properties of the problem [21, 28]. Figure 2 displays the APS in the polar symmetric case in which $\tilde{v}_0 = \tilde{v}_1$. For $\tilde{v}_0 \neq \tilde{v}_1$, on the other hand, the polar symmetry is broken and the lowest APS possesses two local minima instead of the symmetric Mexican hat sombrero shape. In what follows, we will only consider the situation with $\tilde{v}_0 = \tilde{v}_1 \equiv \tilde{v}$, a condition that can be met by adjusting the laser parameters. Thus, in our simulations, the lower APS in momentum space has the familiar sombrero structure.

III. DYNAMICS

We numerically solve the Gross-Pitaevskii equation (6) using the split-operator method [37]. First, we introduce dimensionless variables scaled by the characteristic length and energy given by $l = \sqrt{\hbar/m\omega}$ and $E_c = \hbar\omega$, respectively. The Gross-Pitaevskii equation then attains the form

$$i\frac{\partial}{\partial\tau}\Psi(x, y, \tau) = \left\{ -\frac{1}{2}\left(\frac{\partial^2}{\partial x^2} + \frac{\partial^2}{\partial y^2}\right) + \frac{1}{2}(x^2 + y^2) \right. \\ \left. + v \begin{bmatrix} 0 & -i\frac{\partial}{\partial x} - \frac{\partial}{\partial y} \\ -i\frac{\partial}{\partial x} + \frac{\partial}{\partial y} & 0 \end{bmatrix} \right. \\ \left. + g(|\psi_1(x, y, \tau)|^2 + |\psi_2(x, y, \tau)|^2) \right\} \Psi(x, y, \tau), \quad (11)$$

where

$$x = \frac{\tilde{x}}{l}, \quad y = \frac{\tilde{y}}{l}, \quad \tau = t\omega, \\ v = \frac{\tilde{v}}{E_c}, \quad g = \frac{\tilde{g}}{E_c}. \quad (12)$$

As initial spinor components, we take minimum uncertainty Gaussians

$$\psi_i(x, y, 0) = a_i \left(\frac{1}{\pi\Delta_l^2} \right)^{1/2} e^{-i(p_{x0}x + p_{y0}y)} \\ \times e^{-\frac{(x-x_0)^2 + (y-y_0)^2}{2\Delta_l^2}}, \quad (13)$$

where $|a_i|^2$, normalized as $|a_1|^2 + |a_2|^2 = 1$, determine the initial population in states $|u_i\rangle$ ($i = 1, 2$), Δ_l is the initial wave packet width and x_0, y_0, p_{x0} and p_{y0} are initial averages of positions and momentum. We will choose $\Delta_l = 1$, corresponding to the ground state width of the oscillator potential $\frac{1}{2}(x^2 + y^2)$.

An advantage of utilizing the split-operator method is that the time-dependent solution of the GP equation is automatically obtained in both momentum and position representation. As already pointed out, the effect of the Berry phase is most easily extracted from the momentum wave packets. More precisely, the split-operator method makes use of the fact that for sufficiently short time steps $\delta\tau$, the time-evolution operator can be factorized into one momentum-dependent and one spatially dependent part

$$\Psi(x, y, \tau + \delta\tau) = \exp\left\{-i\left[\frac{1}{2}(p_x^2 + p_y^2) + vp_x\sigma_x + vp_y\sigma_y\right]\delta\tau\right\} \\ \times \exp\left\{-i\left[\frac{1}{2}(x^2 + y^2) + g|\Psi(x, y, \tau)|^2\right]\delta\tau\right\} \\ \times \Psi(x, y, \tau), \quad (14)$$

in the limit $\delta\tau \rightarrow 0$. The first exponent multiplies $\Psi(x, y, \tau)$, then the resulting wave packet is transformed

to momentum space via the fast Fourier algorithm and the second exponent multiplies the momentum wave packet. Finally, the inverse Fourier transform gives the propagated state $\Psi(x, y, \tau + \delta\tau)$. The time step $\delta\tau$ is chosen such that contribution from the non-commuting part, due to factorizing the time-evolution operator, can be safely neglected.

A. Berry phase over short time periods

Let us first examine how the Berry phase of the spinor part of the state behaves when the wave packet encircles the origin $(p_x, p_y) = (0, 0)$. We mainly consider the case with no atom-atom scattering ($g = 0$), and only briefly discuss the $g \neq 0$ case. The spinor state is given by the reduced density operator

$$\rho(t) = P_1(\tau)|u_1\rangle\langle u_1| + P_2(\tau)|u_2\rangle\langle u_2| \\ + C(\tau)|u_1\rangle\langle u_2| + C^*(\tau)|u_2\rangle\langle u_1|, \quad (15)$$

where $P_i(\tau) = \langle\psi_i(\tau)|\psi_i(\tau)\rangle$, $i = 1, 2$, and $C(\tau) = \langle\psi_1(\tau)|\psi_2(\tau)\rangle$ represent the populations and interference, respectively, of the two dark states u_1, u_2 . By writing $\rho(\tau)$ on Bloch form, we identify the time dependent Bloch vector $\mathbf{r}(\tau) = (u(\tau), v(\tau), w(\tau)) = (2\text{Re}C(\tau), -2\text{Im}C(\tau), P_1(\tau) - P_2(\tau))$. We choose an initial wave packet characterized by the parameters $a_1 = -a_2 = 1/\sqrt{2}$, $x_0 = 0, y_0 = -3, p_{x0} = v = 4$, and $p_{y0} = 0$. For this choice, the wave packet will predominantly populate the lower APS and in particular since $p_{x0} = v$ it is located at the minima of the sombrero [40, 41]. Moreover, due to the non-zero $y_0 < 0$, as time evolves it traverses the sombrero minima clockwise. The motion of the Bloch vector representing the spinor state is shown in the upper panel of Fig. (3). Note that $|\mathbf{r}(0)| = 1$ (pure state) since $|\psi_1(0)\rangle = |\psi_2(0)\rangle \equiv |\psi(0)\rangle$, which implies that the initial spinor wave function takes the product form $|\Psi(0)\rangle = |\psi(0)\rangle(|u_1\rangle - |u_2\rangle)/\sqrt{2}$. The Jahn-Teller coupling creates entanglement between the spinor and spatial degrees of freedom when the wave packet evolves, which explains why $|\mathbf{r}(\tau)|$ varies. To compute the evolving Berry phase $\gamma(\tau)$ for this effective non-unitary evolution of the spinor subsystem we write the reduced density operator on spectral form $\rho(\tau) = \sum_{k=1}^2 \lambda_k(\tau)|\varphi_k(\tau)\rangle\langle\varphi_k(\tau)|$ and use [38]

$$\gamma(\tau) = \arg \left[\sum_{k=1}^2 \sqrt{\lambda_k(0)\lambda_k(\tau)} \langle\varphi_k(0)|\varphi_k(\tau)\rangle \right. \\ \left. \times e^{-\int_0^\tau \langle\varphi_k(\tau')|\dot{\varphi}_k(\tau')\rangle d\tau'} \right] \\ = \arg [\langle\varphi_1(0)|\varphi_1(\tau)\rangle] \\ + i \int_0^\tau \langle\varphi_1(\tau')|\dot{\varphi}_1(\tau')\rangle d\tau', \quad (16)$$

where the second equality follows from that $\rho(0)$ is pure (only one $\lambda_k(0)$ is nonzero) and the assumption that $\lambda_1(\tau)$ is the largest eigenvalue over the relevant time interval. Thus, the Berry phase in this case becomes the

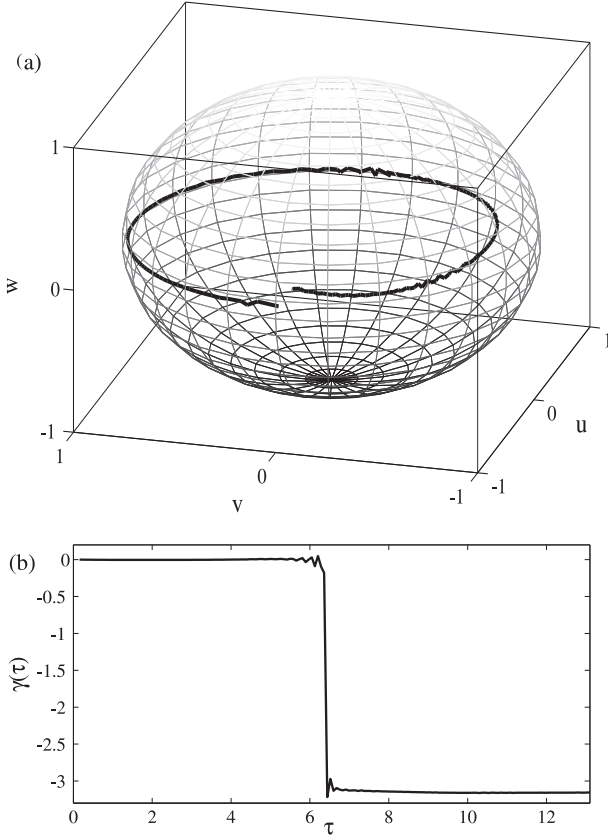


FIG. 3: Bloch vector and corresponding non-cyclic Berry phase for the spinor subsystem with no atom-atom scattering ($g = 0$). The initial state is characterized by the dimensionless parameters $a_1 = -a_2 = 1/\sqrt{2}$, $x_0 = 0$, $y_0 = -3$, $p_{x0} = 4$, and $p_{y0} = 0$.

standard non-cyclic geometric phase [31] for the eigenstate of $\rho(\tau)$ with largest eigenvalue. Here, this phase becomes $-\frac{1}{2}$ times the solid angle $\Omega_{\text{gc}}(\tau)$ enclosed by the path $\tau' \mapsto \mathbf{n}(\tau') = \mathbf{r}(\tau')/|\mathbf{r}(\tau')|$ and the shortest geodesics that connects its end-points $\mathbf{n}(0)$ and $\mathbf{n}(\tau)$. From the upper panel of Fig. 3 we see that $\Omega_{\text{gc}}(\tau) \approx 0$ for the first half of the path, and $\Omega_{\text{gc}}(\tau) \approx 2\pi$ for the second half. Thus, we expect $\gamma(\tau) = -\frac{1}{2}\Omega_{\text{gc}}(\tau)$ to make a π -jump at half the period of the motion. This behavior of the non-cyclic Berry phase in the $E \otimes \varepsilon$ Jahn-Teller system has been examined in the literature [39] and is verified in the lower panel of Fig. 3. Note the wiggles in the vicinity of the phase jump which are caused by small non-adiabatic effects in the wave packet motion.

To extract measurable effects of the non-zero Berry phase we need the wave packet to self-interfere. To this end, we assume as above $a_1 = -a_2 = 1/\sqrt{2}$, $x_0 = y_0 = p_{y0} = 0$, $p_{x0} = v$, while now $y_0 = 0$. Thus, the momentum wave packet has no initial velocity, so for zero atom-atom scattering corresponding to $g = 0$, the wave packet starts to spread around the minima of the sombrero. We emphasize that this spreading takes place in the momentum wave packet Φ , and is driven by the un-

certainty in the spatial coordinates. Thus, such spreading is only possible since we consider a harmonically trapped condensate, contrary to Refs. [11, 13] where no trapping was taken into account. For positive g , the interaction is repulsive which tends to increase the spreading of the Ψ wave packet while slowing down the Φ wave packet broadening. The opposite occurs for attractive interaction. Consequently, no overall spreading in Φ takes place if g is large and negative.

We assume a g such that for sufficiently long times, Φ has spread noticeable compared to its initial state. Then, after some time τ_{col} , the wave packet has expanded a distance $2\pi\rho_{\text{min}}$, where ρ_{min} is the radii of the minima of the sombrero. The wave packet tails will then start to overlap and cause a self-interference pattern. It was shown in Ref. [41] that $\tau_{\text{col}} = 2\pi v$, a result which applies to the present model in the absence of atom-atom interaction. As the structure of the interference depends on the wave packet phases, both the dynamical phase and the Berry phase will be manifested in its shape.

In order to describe the effect of the Berry phase γ , the dynamics rendered by the Gross-Pitaevskii equation (11) will be compared with the dynamics of an adiabatic Hamiltonian possessing the same lower APS but lacking any Berry phase. As mentioned above, for the particular choice of parameters, $x_0 = y_0 = p_{y0} = 0$, $p_{x0} = v$, $\Delta_l = 1$ and $a_1 = -a_2 = 1/\sqrt{2}$, the wave packet evolution takes place essentially on the lower APS. We therefore make a *single surface approximation* [42], writing an effective Hamiltonian as

$$H_S = \frac{x^2}{2} + \frac{y^2}{2} + V_{\text{ad}}^-, \quad (17)$$

which follows from the adiabatic transformation defined in Eq. (9) and by ignoring the Berry vector potential $\vec{A}(\vec{p}) = (-p_y, p_x)/(2\vec{p}^2)$ as well as the Born-Huang scalar potential $1/(8\vec{p}^2)$ [43, 44]. Ignoring \vec{A} implies that no Berry phase arises when the wave packet encircles the CI at the origin in momentum space [41]. On the other hand, the dynamical phases acquired in the two models are almost identical, since the effect of the Born-Huang potential is small for the type of evolution that is considered here. In order to identify the consequences of the Berry phase on the characteristics of the two systems, it is therefore convenient to analyze the wave packet evolution in the two respective models. Figure 4 depicts, for $g = 0$ (a)-(f) and $g \neq 0$ (g)-(l), the momentum distribution

$$|\Phi(p_x, p_y, \tau_f)|^2 = |\phi_1(p_x, p_y, \tau_f)|^2 + |\phi_2(p_x, p_y, \tau_f)|^2 \quad (18)$$

from our numerical propagation of the wave packet after a time $\tau_f = \tau_{\text{col}}$ when self-interference has been clearly manifested. Similar figures were presented in Refs. [40, 41] for different systems. The upper left and lower plots are obtained from the full system evolution governed by Eq. (11), while the upper right plots are the results achieved using the single surface approximation (17). The effect of the Berry phase is evident;

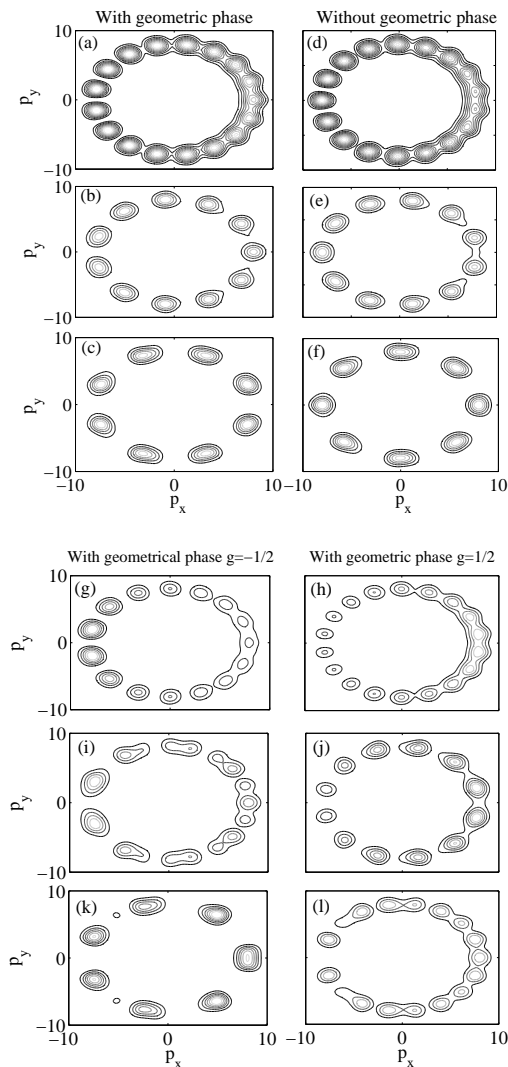


FIG. 4: Snapshots at times $\tau = \tau_{\text{col}}/2, 3\tau_{\text{col}}/4, \tau_{\text{col}}$ of the momentum distribution Eq. (18) after the initial wave packet has spread out around the minima of the sombrero potential. Upper left plot presents the result with a Berry phase present and upper right one without it. Here, the dimensionless parameters are $v = 8$, $g = 0$, and $\tau_{\text{col}} = 16\pi$. The lower plots (g)-(l) display the results from having a non-zero scattering amplitude ($g \neq 0$), essentially affecting the rate of wave packet broadening. Again, $v = 8$ and $\tau_{\text{col}} = 16\pi$.

it is especially found that a node/antinode appears at $p_x < 0, p_y = 0$ in the cases with/without Berry phase. The location of this node/antinode persists throughout the evolution. The total number of nodes/antinodes, on the other hand, changes with time, which was demonstrated in Ref. [41].

The wave packet spreading, as it evolves along the minima of the sombrero, takes place relatively far from the CI for the parameters of the above examples. In other words, the dynamics is predominantly adiabatic. However, the concept of adiabaticity in non-linear systems is highly non-trivial since the superposition principle and

orthonormality of quantum states are no longer applicable [45]. As the strength of the non-linearity is increased, the constraints for adiabatic evolution are in general strengthened. This has been studied in numerous papers, mainly focusing on various curve-crossing models [46, 47], but also on the Berry phase [48]. In the current system and for the parameters considered, non-linearity manifests itself in the characteristic time scales rather than on the Berry phase effect. This is illustrated in Fig. 4 (g)-(l) where the Berry phase induced node at $p_x < 0, p_y = 0$ is invariant. The number of nodes, however, depends on the non-linearity coefficient g , and consequently the characteristic times are g -dependent. This result may be taken as further evidence of the conjectured robustness of Berry phase effects to various kinds of errors and therefore of the potential utility of such phases in the implementation of robust quantum computers [49]. The persistence of the Berry phase effect due to non-linearity was also demonstrated in the model of Ref. [30]. We should point out that in other situations than the one considered in this work, namely when the wave packet dynamics takes place at the CI, the effect of the non-linearity is supposed to become important. It is known that non-linearity of the periodic Gross-Pitaevskii equation can bring about loops at the Brillouin center and at its edges [47], and similar loops might be formed at the CI. This, however, goes beyond the scope of this work.

To experimentally extract the impact of the Berry phase, a time-of-flight measurement can be implemented by switching off the trapping potential and the external lasers to let the condensate ballistically evolve before detecting it. In Fig. 5 we show an example of such a ballistic expansion of the wave packet distributions $|\Psi(x, y, \tau)|^2$ after it has been released from the trap. The parameters are the same as in Fig. 4 (a)-(f) and the release time $\tau_r = \tau_{\text{col}} = 16\pi$ corresponds to Fig. 4 (c) and (f). The form of the momentum distributions, as shown in Fig. 4 (c) and (f), are clearly embodied in the position distribution. Assuming a typical trapping potential frequency $\omega/2\pi = 40$ Hz, the characteristic time scale is 4 ms. Hence, the time-of-flight of Fig. 5 is around 10 ms. This is of the same order as in common time-of-flight measurements of condensates in optical lattices [50]. Moreover, the interaction times of Fig. 4 are of the order of 50-100 ms for this particular trapping potential frequency. Quantum phase diffusion of the condensate [51], arising from quantum fluctuations beyond the mean field description, will most likely decrease the visibility of the interference pattern. However, phase coherence of 50 ms has been observed experimentally [52], and at these time scales the Berry phase has already been manifested in the interference pattern.

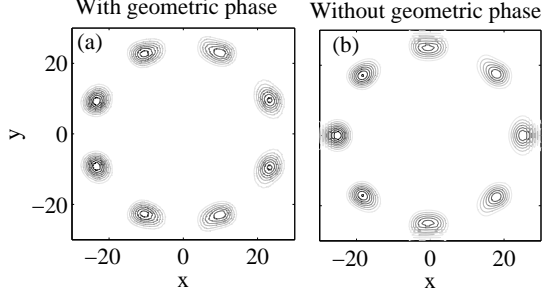


FIG. 5: The position distributions after ballistic expansion. As in Fig. 4, the left and right plots represent the results with and without a Berry phase. The dimensionless parameters are the same as in Fig. 4 (a)-(f), and the time-of-flight duration is $\tau_{\text{tof}} = \pi$.

B. Impact of the Berry phase over long times

The time scale τ_{col} for self-interference of the wave packet to be established, characterizes a collapse period. For longer time periods, the number of wave packet maxima/minima of Fig. 4 decrease to finally a single maximum is recovered signaling a full or half revival [41, 53]. The formation of the wave packet maxima/minima is indeed highly dependent on the Berry phase. To verify this, we define the number of phonon excitations in the two modes

$$n_i \equiv \frac{\langle p_i^2 \rangle}{2} + \frac{\langle i^2 \rangle}{2}, \quad i = x, y. \quad (19)$$

This quantity is depicted in Fig. 6, where the upper three plots are found using the full Hamiltonian Eq. (11) and the corresponding single surface results are presented in the lower three plots. In (a) and (d) $g = 0.25$, in (b) and (e) $g = 0$ and finally in (c) and (f) $g = -0.25$. Interestingly, at around $\tau \approx 200$ the population is swapped between the two phonon modes in the case of Berry phase (a)-(c) but not when the Berry phase is absent (d)-(f). At times $\tau \approx 400$ does a half revival occur [41]. The figure also gives a measure on how the non-linear interaction affects the time scales: positive g increases while negative g decreases the time periods over which the system characteristics are established.

C. Non-Abelian manifestation

We note that the Hamiltonian of Eq. (11) can be written, for $g = 0$, as

$$H_{\text{eff}} = \frac{(\vec{p} - \vec{A})^2}{2} + \frac{(x^2 + y^2)}{2}, \quad (20)$$

where $\vec{p} = (p_x, p_y)$ and $\vec{A} = (A_x, A_y) = v(\sigma_x, \sigma_y)$. The gauge vector potential \vec{A} has a matrix form due to the

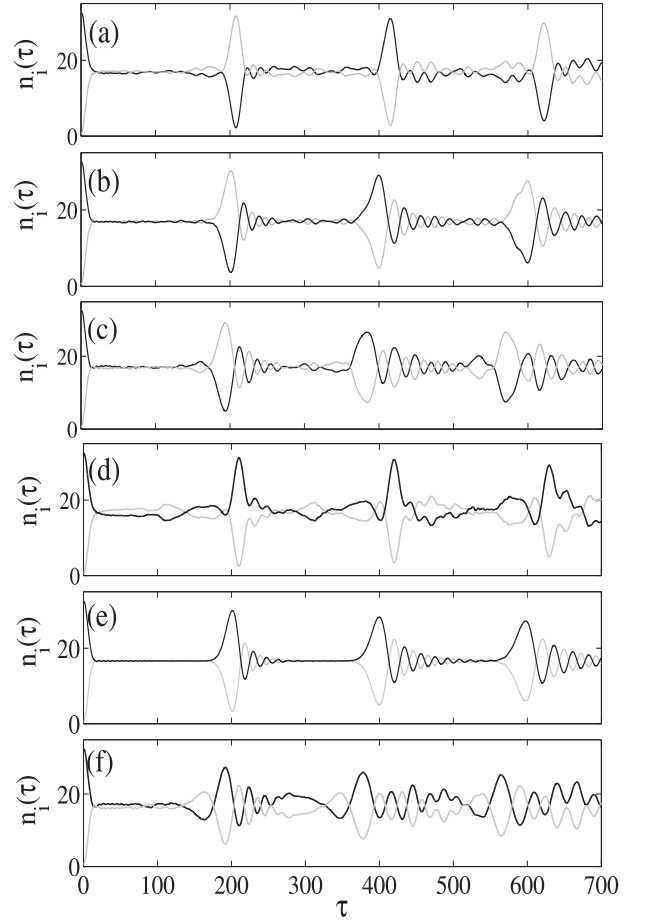


FIG. 6: The average number of phonon excitations n_i $i = x$ (black curve) and $i = y$ (gray curve) as a function of time with (a)-(c) and without (d)-(f) Berry phase. Here $g = 0.25$ (a) and (d), $g = 0$ (b) and (e) and $g = -0.25$ (c) and (f). The rest of the dimensionless parameters are as in Fig. 4.

internal two-level structure of our system. The fact that $[A_x, A_y] \neq 0$ implies that the gauge field has a non-Abelian character. As pointed out in Ref. [11], encircling the CI clockwise or anti-clockwise is supposed to bring about different system evolution despite the polar symmetry of the system. More precisely, after one round-trip of the CI, the populations $P_i(\tau)$ of the two degenerate dark states $|u_i\rangle$ ($i = 1, 2$) depend on the direction the wave packet traversed the minima of the sombrero. We demonstrate this in Fig. 7 by displaying the time evolution of the populations for approximately one round-trip clockwise (a) or anti-clockwise (b). We find that the progression of $P_1(\tau)$ and $P_2(\tau)$ is interchanged between clockwise or anti-clockwise wave packet evolution, and therefore revealing the underlying non-Abelian structure. From the right plots, zooming in on the short time evolution, it is clear that the initial population is equally balanced between the two internal states, i.e., $|a_1|^2 = |a_2|^2 = 1/2$.

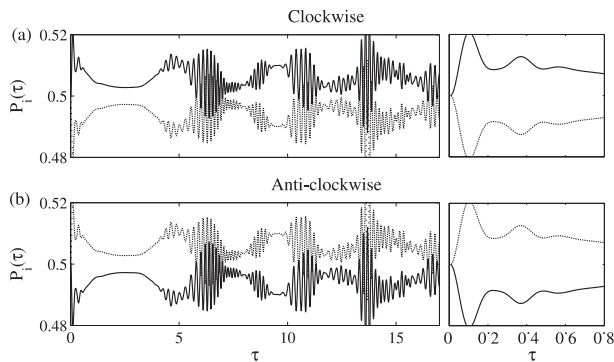


FIG. 7: Populations $P_i(\tau)$ of the dark states $|u_i\rangle$ for clockwise and anti-clockwise evolution of the wave packet around the CI. Solid lines show the population of the state $|u_2\rangle$ and dashed lines the population of $|u_1\rangle$. The figures to the right display the short time behavior, which evidence that initially both internal states are equally populated $P_1(0) = P_2(0) = 1/2$. The initial state are as in the previous figures ($p_{x0} = v$, $\Delta_I = 1$ and $a_1 = -a_2 = 1/\sqrt{2}$) and $y_0 = 3$ (a) or $y_0 = -3$ (b). The other dimensionless parameters are $g = 0$ and $v = 4$.

IV. CONCLUSIONS

We have analyzed a spin-orbit coupled BEC system, emphasizing on the Berry phase and non-Abelian gauge structures and their importance for the dynamics. We have demonstrated that the non-Abelian structure associated with the center of mass position of the atoms

is mirrored in the momentum space wave packet interference as a Berry phase. This Berry phase has been computed and its effect has been identified by comparing the dynamics of the full system with one possessing the same adiabatic potential energy surface but lacking the Berry phase. A time-of-flight measurement would therefore directly bring out the presence of such a phase. Over longer time periods, a periodic Berry phase dependent interchange of excitations between the x and y directions was demonstrated. We have also shown how the non-Abelian aspect of the model system is manifested in the wave packet dynamics in position space by propagating in different directions around the CI.

It is worth mentioning that the results are not restricted to a spin-orbit coupled BEC, but can equally well be applied to single trapped ions [54]. Using the same laser and atomic configurations, the dynamics is governed by Eq. (11) letting $g \rightarrow 0$. Berry phases have been discussed in such systems [55], but those settings are different from the one considered here.

Acknowledgments

JL acknowledge support from the MEC program (FIS2005-04627) and wishes to thank Prof. Stig Stenholm for fruitful discussions. ES acknowledge support from the Swedish Research Council.

-
- [1] M. H. Anderson, J. R. Ensher, M. R. Matthews, C. E. Wieman, and E. A. Cornell, *Science* **269**, 198 (1995); K. B. Davis, M.-O. Mewes, M. R. Andrews, N. J. vanDruten, D. S. Durfee, D. M. Kurn, and W. Ketterle, *Phys. Rev. Lett.* **75**, 3969 (1995).
 - [2] M. Lewenstein, A. Sanpera, V. Ahufinger, B. Damski, A. Sen, and U. Sen, *Adv. Phys.* **56**, 243 (2007).
 - [3] Y. Ohashi and A. Griffin, *Phys. Rev. Lett.* **89**, 130402 (2002); T. Bourdel, L. Khaykovich, J. Cubizolles, J. Zhang, F. Chevy, M. Teichmann, L. Tarruell, S. J. J. M. F. Kokkelmans, and C. Salomon, *Phys. Rev. Lett.* **93**, 050401 (2004).
 - [4] C. K. Law, H. Pu, and N. P. Bigelow, *Phys. Rev. Lett.* **81**, 5257 (1998); D. M. Stampfer-Kurn, M. R. Andrews, A. P. Chikkatur, S. Inouye, H.-J. Meisner, J. Stenger, and W. Ketterle, *Phys. Rev. Lett.* **80**, 2027 (1998).
 - [5] R. Dum and M. Olshanii, *Phys. Rev. Lett.* **76**, 1788 (1996); P. M. Visser and G. Nienhuis, *Phys. Rev. A* **57**, 4581 (1998); G. Juzeliunas and P. Öhberg, *Phys. Rev. Lett.* **93**, 033602 (2004); P. Zhang, Y. Li, and C. P. Sun, *Eur. Phys. J. D* **36**, 229 (2005); G. Juzeliunas, P. Öhberg, J. Ruseckas, and A. Klein, *Phys. Rev. A* **71**, 053614 (2005); X.-J. Liu, X. Liu, L. C. Kwek, and O. H. Oh, *Phys. Rev. Lett.* **98**, 026602 (2007); M. Cheneau, S. P. Rath, T. Yefsah, K. J. Günter, G. Juzeliunas, and J. Dalibard, *Eur. Phys. Lett.* **83**, 60001 (2008).
 - [6] K. J. Günter, M. Cheneau, T. Yefsah, S. P. Rath, and J. Dalibard, *Phys. Rev. A* **79**, 011604(R) (2009).
 - [7] S. K. Dutta, B. K. Teo, and G. Raithel, *Phys. Rev. Lett.* **83**, 1934 (1999); Y.-J. Lin, R. L. Compton, A. R. Perry, W. D. Phillips, J. V. Porto, and I. B. Spielman, *Phys. Rev. Lett.* **102**, 130401 (2009).
 - [8] J. Ruseckas, G. Juzeliunas, P. Öhberg, and M. Fleischhauer, *Phys. Rev. Lett.* **95**, 010404 (2005).
 - [9] R. G. Unanyan, B. W. Shore, and K. Bergmann, *Phys. Rev. A* **59**, 2910 (1998).
 - [10] S.-L. Zhu, H. Fu, C.-J. Wu, S.-C. Zhang, and L.-M. Duan, *Phys. Rev. Lett.* **97**, 240401 (2006).
 - [11] A. Jacob, P. Öhberg, G. Juzeliunas, and L. Santos, *Appl. Phys. B* **89**, 439 (2007).
 - [12] G. Juzeliunas, J. Ruseckas, M. Lindberg, L. Santos, and P. Öhberg, *Phys. Rev. A* **77**, 011803(R) (2008); M. Merkl, E. F. Zimmer, G. Juzeliunas, and P. Öhberg, *Europhys. Lett.* **83**, 54002 (2008); G. Juzeliunas, J. Ruseckas, A. Jacob, L. Santos, and P. Öhberg, *Phys. Rev. Lett.* **100**, 200405 (2008).
 - [13] J. Y. Vaishnav and C. W. Clark, *Phys. Rev. Lett.* **100**, 153002 (2008).
 - [14] T. D. Stanescu, C. Zhang, and V. Galitski, *Phys. Rev. Lett.* **99**, 110403 (2007).
 - [15] J. Y. Vaishnav, J. Ruseckas, C. W. Clark, and G. Juzeliunas, *Phys. Rev. Lett.* **101**, 265302 (2008).

- [16] L.-H. Lu and Y.-Q. Li, Phys. Rev. A **76**, 023410 (2007).
- [17] T. D. Stanescu, B. Anderson, and V. Galitski, Phys. Rev. A **78**, 023616 (2008).
- [18] A. Jacob, P. Öhberg, G. Juzeliunas, and L. Santos, New J. Phys. **10**, 045022 (2008).
- [19] V. Pietilä and M. Möttönen, Phys. Rev. Lett. **102**, 080403 (2009).
- [20] M. Baer, *Beyond Born-Oppenheimer* (Wiley, New York, 2006).
- [21] C. A. Mead, Rev. Mod. Phys. **64**, 51 (1992).
- [22] C. A. Mead and D. G. Truhlar, J. Chem. Phys. **70**, 2284 (1979); C. A. Mead, Chem. Phys. **49**, 23 (1980).
- [23] M. V. Berry, Proc. R. Soc. London Ser. A **392**, 45 (1984).
- [24] C. L. Kane and E. J. Mele, Phys. Rev. Lett. **95**, 226801 (2005); Y. B. Zhang, Y. W. Tan, H. L. Stormer, and P. Kim, Nature **438**, 201 (2005); K. S. Novoselov, A. K. Geim, S. V. Morozon, D. Jiang, M. I. Katsnelson, I. V. Grigorieva, S. V. Dubonos, and A. A. Firsov, Nature **438**, 197 (2005).
- [25] A. D. Dudarev, R. B. Diener, I. Carusotto, and Q. Niu, Phys. Rev. Lett. **92**, 153005 (2004); S. L. Zhu, B. G. Wang, and L. M. Duan, Phys. Rev. Lett. **98**, 260402 (2007).
- [26] H. C. Longuet-Higgins, U. Öpik, M. H. L. Pryce, and R. A. Sack, Proc. R. Soc. London Ser. A **244**, 1 (1958).
- [27] D. R. Yarkony, Rev. Mod. Phys. **68**, 985 (1996).
- [28] A. Bohm, A. Mustafazadeh, H. Kuizumi, Q. Niu, and J. W. Zwanziger, *Geometric Phase in Quantum Systems* (Springer, Berlin, 2003).
- [29] I. Fuentes-Guridi, J. Pachos, S. Bose, V. Vedral, and S. Choi, Phys. Rev. A **66**, 022102 (2002); E. I. Duzzioni, L. Sanz, S. S. Mizrahi, and M. H. Y. Moussa, Phys. Rev. A **75**, 032113 (2007).
- [30] Z. D. Chen, J. Q. Liang, S. Q. Shen, and W. F. Xie, Phys. Rev. A **69**, 023611 (2004).
- [31] J. Samuel and R. Bhandari, Phys. Rev. Lett. **60**, 2339 (1988); N. Mukunda and R. Simon, Ann. Phys. (N.Y.) **228**, 205 (1993).
- [32] J. Larson and S. Stenholm, Phys. Rev. A **73**, 033805 (2006).
- [33] Y. A. Bychkov and E. I. Rashba, J. Phys. C **17**, 6039 (1984).
- [34] S.-R. E. Yang and N. Y. Hwang, Phys. Rev. B **73**, 125330 (2006); P. Pietiläinen and T. Chakroborty, Phys. Rev. B **73**, 155315 (2006).
- [35] H. Tütüncüler, R. Koc, and E. Olgar, J. Phys. A: Math. Gen. **37** 11431 (2004).
- [36] H. Feshbach, Ann. Phys. **5**, 337 (1958); E. Tsesinga, B. J. Verhaar, and H. T. C. Stoof, Phys. Rev. A **47**, 4114 (1993); C. Chin, R. Grimm, P. Julienne, and E. Tsesinga, arXiv:0812.1496.
- [37] M. D. Flei, J. A. Fleck, and A. Steiger, J. Comp. Phys. **47**, 412 (1982).
- [38] D. M. Tong, E. Sjöqvist, L. C. Kwek, and C. H. Oh, Phys. Rev. Lett. **93**, 080405 (2004).
- [39] E. Sjöqvist and M. Hedström, Phys. Rev. A **56**, 3417 (1997); R. Englman, A. Yahalom, and M. Baer, Eur. Phys. J. D **8** 1 (2000).
- [40] J. Schön and H. Köppel, J. Chem. Phys. **103**, 9292 (1995); J. Schön and H. Köppel, J. Chem. Phys. **108**, 1503 (1998).
- [41] J. Larson, Phys. Rev. A **78**, 033833 (2008).
- [42] R. Baer, D. M. Charutz, R. Kosloff, and M. Baer, J. Chem. Phys. **105**, 9141 (1991); S. Adhikari and G. D. Billing, J. Chem. Phys. **111**, 40 (1999).
- [43] M. Born and K. Huang, *Dynamical theory of crystal lattices* (Clarendon, Oxford, 1954), pp. 406-407.
- [44] M.V. Berry and R. Lim, J. Phys. A **23**, L655 (1990).
- [45] J. Liu, B. Wu, and Q. Niu, Phys. Rev. Lett. **90**, 170404 (2003).
- [46] B. Wu and Q. Niu, Phys. Rev. A **61**, 023402 (2000); V. A. Brazhnyi and V. V. Konotop, Mod. Phys. Lett. B **18**, 627 (2004).
- [47] M. Machholm, C. J. Pethick, and H. Smith, Phys. Rev. A **67**, 053613 (2003).
- [48] B. Wu, J. Liu, and Q. Niu, Phys. Rev. Lett. **94**, 140402 (2005); X. X. Yi, X. L. Huang, and W. Wang, Phys. Rev. A **77**, 052115 (2008).
- [49] J. A. Jones, V. Vedral, A. Ekert, and G. Castagnoli, Nature **403**, 869 (2000); W. Xiang-Bin and M. Keiji, Phys. Rev. Lett. **87**, 097901 (2001); D. Leibfried, B. DeMarco, V. Meyer, D. Lucas, M. Barrett, J. Britton, W. M. Itano, B. Jelenkovic, C. Langer, T. Rosenband, and D.J. Wineland, Nature **422**, 412 (2003).
- [50] F. Gerbier, A. Widera, S. Fölling, O. Mandel, T. Gericke, and I. Bloch, Phys. Rev. Lett. **95**, 050404 (2005).
- [51] M. Lewenstein and L. You, Phys. Rev. Lett. **77**, 3489 (1996).
- [52] D. S. Hall, M. R. Matthews, C. E. Wieman, and E. A. Cornell, Phys. Rev. Lett. **81**, 1543 (1998); M. Albiez, R. Gati, J. Fölling, S. Hunsmann, M. Cristiani, and M. K. Oberthaler, Phys. Rev. Lett. **95**, 010402 (2005).
- [53] R. W. Robinett, Phys. Rep. **392**, 1 (2004); E. Romera and F. de los Santos, Phys. Rev. Lett. **99**, 263601 (2007).
- [54] D. Leibfried, R. Blatt, C. Monroe, and D. J. Wineland, Rev. Mod. Phys. **75**, 281 (2003).
- [55] I. Fuentes-Guridi, S. Bose, and V. Vedral, Phys. Rev. Lett. **85**, 5018 (2000); X.-D. Zhang, Z. D. Wang, L.-B. Hu, Z.-M. Zhang, and S.-L. Zhu, New J. Phys. **10**, 043031 (2008).